Available online at www.sciencedirect.com
ScienceDirect
Journal of Sound and Vibration 311 (2008) 109–132
JOURNAL OF SOUND AND VIBRATION
www.elsevier.com/locate/jsvi

Vibration and current transient monitoring for gearbox fault detection using multiresolution Fourier transform

Chinmaya Kar[a], A.R. Mohanty[b,*]

[a]*Remote Prognostics Lab, General Electric Global Research, 122, EPIP, Bangalore 560066, India*
[b]*Mechanical Engineering Department, Indian Institute of Technology, Kharagpur (WB)—721 302, India*

Received 22 August 2007; received in revised form 22 August 2007; accepted 24 August 2007
Available online 23 October 2007

Abstract

This paper deals with an experimental investigation of fault diagnosis in a multistage gearbox under transient loads. An induction motor drives the multistage gearbox, which is connected to a DC generator for loading purpose. The signals studied are the vibration transients, recorded from an accelerometer fitted at the tail-end bearing of the gearbox; and the current transients drawn by the induction motor. Three defective cases and three transient load conditions are investigated. Advanced signal processing techniques such as discrete wavelet transform (DWT) and a corrected multiresolution Fourier transform (MFT) are applied to investigate the vibration and current transients. It is observed from the vibration transients that the load removal is a high-frequency phenomenon. With increase in defect severity, not only the defective gear mesh frequency gains energy, but also large impact energy appears in low-frequency regions. Whereas in the current transients, though load removal is a low-frequency phenomenon, a very small transient is observed at high-frequency regions for defective gears. With increase in defect severity, energy is distributed to the sidebands of the gear mesh frequency across supply line frequency. A statistical feature extraction technique is proposed in order to find a trend in detection of defects. A condition monitoring scheme is devised that can facilitate in monitoring vibration and current transients in the gearbox with simultaneous presence of transient loads and defects.

1. Introduction

In a gearbox, presence of internal exciting forces such as mesh stiffness variation, friction force variation, transmission error, etc., and defects in the gears lead to non-stationary vibration signals [1,2]. Generally, in all these analysis, load is considered to be constant. Recent articles have also investigated various loads such as cyclic and non-cyclic stationary load [1,2], and varying load [3]. These applied loads meet the real-life situation, where there is a large-scale fluctuation in load observed in gearboxes. Stander et al. [1,2] have applied cyclic and non-cyclic stationary loads such as constant, sine, square and chirp to a single-stage spur gear system. They applied smoothed pseudo Wigner–Ville distribution (SPWVD) [1,2], order tracking and time domain averaging techniques to distinguish faults in the gears. Byder and Ball [3] have performed experiments to detect faults with 25% increments of load from no load to full rated load using instantaneous power spectrum. In a recent article, Bonnardot et al. [4] have applied a method of order tracking that can be

*Corresponding author. Tel.: +91 3222 282944; fax: +91 3222 255303.
E-mail address: amohanty@mech.iitkgp.ernet.in (A.R. Mohanty).

0022-460X/$ - see front matter © 2007 Elsevier Ltd. All rights reserved.
doi:10.1016/j.jsv.2007.08.023

Nomenclature

A_{sM}	magnetizing component of current
A_{sT}	torque producing component of current
b	face width of the gear and pinion
f	width of the contact zone
f_e	supply line frequency
f_{ecc}, f_{load}	frequencies due to rotor eccentricity and load torque, respectively
f_i	some important widths in the base/action plane, $i = 1,2$
fr_i	the ith defect frequency with n-number of defect frequencies
I_0	average current drawn by the supply line frequency
I_s	stator current of the induction motor
L_i	contact length of pinion for ith line
L^{d0}	total length of contact lines in all the contact zones for defect-free case
L^{di}	total length of contact lines in all the contact zones for ith defective case, $i = 1$, 2, and 3.
m	any positive integer
n	number of teeth in the pinion
p	number of pole in the induction motor
P_t	transverse pitch of the gear system, respectively
r_a, r	addendum and pitch circle diameter of pinion (2nd counter gear in this paper)
R_a, R	addendum and pitch circle diameter of gear (2nd main gear in this paper)
s	slip in the motor
t	time
v	velocity at pitch point
w_a	window w at a scale a
$\hat{x}$	MFT coefficients
α	helix or spiral angle of the gear and pinion
α_b	base helix angle
δL^{di}	percentage loss in contact lines for ith defective case, $i = 1,2$, and 3.
λ, i	flux linkage and current, respectively along quadrature (qs) and direct (ds) axes of stator with corresponding subscripts
τ	time translation
ϕ	pressure angle of the gear and pinion
ϕ_0, ϕ_i	the phase difference for f_e and fr_i, respectively.

used in analyzing the acceleration signal when there is a small fluctuation in speed. The effect of transient load i.e. sudden application or removal of load during the operation has been rarely reported.

A number of authors have already devoted their attention in monitoring vibration signal under steady load conditions. Staszweski and Tomilnson in a series of papers [5–7] have applied Wigner–Ville distribution (WVD), short-time Fourier transform (STFT) and wavelet transform (WT) to vibration signals of a spur gear pair at steady loads in order to detect various fault advancements. Wang and McFadden [8,9] have applied STFT and WT to diagnose pitting, spalling and root crack in gears. Stander et al. [2] have observed that order tracking mainly deals with spectral smearing due to fluctuating speed conditions. Some other signal processing techniques, which have been applied for analyzing vibration signals have been reviewed in Refs. [10,11]. Dalpiaz et al. [12], Byder and Ball [13], and Gaborson [14] have concluded that WT is the best-suited technique to analyze vibration signals for fault detection in a gearbox.

In many instances, an induction motor is used to drive a gearbox. And any fluctuating or transient load in the gearbox produces transients in the current drawn by the induction motor. Monitoring stator current transients during the starting of the induction motor is a prevalent technique for fault detection in induction motor [15–18] and its bearings [19]. Douglas et al. [16,17] have combined all three phases of current transients of the induction motor by Park's vector approach and applied discrete wavelet transform (DWT) to detect broken rotor bar. Eren and Devany [19] used wavelet packet analysis in order to detect defects in a bearing. In Ref. [10], the authors have detected defects in gearbox by applying DWT to the current transients due to removal of load. It is observed that under defective conditions, low energy transients appear in the high-frequency region; containing sidebands of gear mesh frequencies (GMF) across the supply line frequency. It is also shown that continuous wavelet transform (CWT) is not effective to trace such small transients in the current signal. There is also one literature [20] where the stator-induced voltage is investigated after switching off the induction motor. For current transient analysis, generally DWT [10,16–18] is preferred using

duabechies (Db) orthogonal wavelet. Douglas and Pillay [17] have compared the effects of various wavelets and recommended the 'Db8' wavelet, which had been used by the authors in Ref. [10].

Spectrum analysis [21,22], demodulation [23], WT [10,21,23] and corrected multiresolution Fourier transform (MFT) [23] have already been applied for investigating current signatures under steady loads. Following are some important observations on the analysis of current signatures. Yacamini et al. [21] have observed that low frequencies can easily be detected in the spectrum and the scalogram, as sidebands of supply line frequency, whereas high-frequency components are difficult to be traced. Ball et al. [22] could not monitor frequencies higher than 2nd harmonics of supply line frequency and also concluded that the fault detection is very difficult at load lesser than 25% of the rated load. Schoen and Habetler [24] experienced difficulty in measuring frequencies higher than 4th harmonics of supply line frequency. In a very recent paper, Henao et al. [25] have detected broken rotor bar by focusing around 5th harmonics of supply line frequency. But, the authors [10] have detected sidebands of supply line frequency due to defects in a multistage helical gearbox, which are in between 12th and 20th harmonics of supply line frequency, at 15% of the rated load.

Defect severity in gears has been subjective in the literature, depending upon the amount of load applied with respect to the rated load of the gearbox, types of gear such as spur or helical, and number of stages of gears. A particular defect such as one tooth missing may not be considered as a severe defect in a helical gear because of very high contact ratio (and hence large number of contact lines), but may be considered as a severe defective case in a spur gear. Furthermore, the number of contact lines is much higher for multistage gears under synchro-meshed condition. Diagnosis of defect is easier in a gear with a rated or over-rated load than an under-rated load. Staszweski and Tomilnson [5–7] have classified the defects in gears into tooth breakage, tooth root crack, and surface wear and spalling. In their paper, they investigated defects in a single-stage spur gear with maximum of two broken teeth under 70% of maximum load. Byder and Ball [13] have studied a 2-stage helical gear with removal of one tooth and then further increment removal of adjacent teeth with an applied load torque of 260 N m. Moreover, root crack of 1–4 mm depth have been investigated. Wang and McFadden [8] have investigated spalls in one tooth of the three-stage double helical gear. In another paper [9], they have detected root crack in bevel gear of a helicopter gearbox under very high load. Dalpiaz et al. [12] have detected surface crack in 2-stage spur gears under a load torque of 385 N m. Stander et al. [1] have detected surface removal and root crack in spur gear of 25% and 50% severity under maximum of load torque of 16 N m. In a recent paper [2], they have applied maximum load torque of 14.7 N m to a helical gearbox with a rated load torque of 20 N m to detect tooth surface wear of 100–300 μm. Zheng et al. [26] have investigated a helical gear system with four consecutive teeth broken in seeded manner i.e. the maximum breakage 1st tooth broken completely, next tooth is broken 75%, 3rd tooth is broken to 50%, 4th tooth is broken to 25%.

This paper aims at devising a monitoring scheme that can

1. detect defects in a gearbox using both vibration and current transients,
2. compare the vibration transients and the current transients for a particular defect condition in the gearbox,
3. investigate the effects of various defects on these transients,
4. use a single analysis technique (i.e. MFT) for detecting defects in the gearbox irrespective of monitoring techniques (vibration and current analysis), and
5. establish the difference between the effect of load and defects.

A multistage gearbox test rig; described in Refs. [10,11], is used in the present study. The test setup comprises of a multistage gearbox, driven by an induction motor and loaded by a generator. The gearbox is an automotive transmission gearbox with three gears, such as 2nd, 3rd, and 4th gears, under synchro-meshed condition, as illustrated in Fig. 1. Three types of artificially introduced defect and three cases of transient load conditions are discussed in the paper. Both vibration and current transients are investigated using DWT and MFT.

2. Theory

2.1. Severity of defects

The line diagram of the multistage gearbox is illustrated in Fig. 1. It has three gears; 2nd, 3rd, and 4th gears, under synchro-meshed condition. The artificial defects introduced in the gearbox are shown in Table 1.

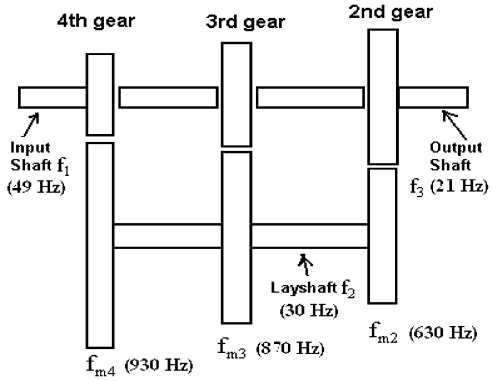

Fig. 1. Line diagram of the multistage gearbox.

Table 1
Types of artificial defects and applied load conditions introduced in gears

Sl. no.	Helical gear	Type of defect	Steady loads (kW)	Load transients (kW)
1	–	No defect (d0)	0	1.875
2	2nd gear (main)	1 tooth broken ($d1$)	1.875	3.75
3	2nd gear (main)	2 teeth broken ($d2$)	3.75	5.625
4	2nd gear (lay shaft)	2 teeth broken ($d3$)	5.625	

These are one tooth and two teeth missing in 2nd main gear and two teeth missing in 2nd counter gear. These defects are termed as $d1$, $d2$, and $d3$ defective cases, respectively, and the defect-free case is termed as $d0$ condition. In this section, an endeavor is made to quantify the severity of defects taken in this paper by considering the loss of length of contact lines as a parameter.

Fig. 2a illustrates a single-stage helical gear system, where the contact zone is the area bounded by the intersection of addendum circles of gear and pinion with the line of action. The line of action is the common tangent to the base circles of the gear and the pinion. The length of the contact zone depends on the addendum and pitch circle diameters of gear (R_a and R) and pinion (r_a and r) and the pressure angle (Φ). Its width is the width of the meshing gear pair (b). Each meshing teeth pair will form a contact line in the contact zone. The contact ratio of the gears is 2.9, hence at any point of time, there will be 2–3 number of contact lines in the meshing or contact zone. In a three-stage synchro-meshed helical gear system with a layshaft, there will be simultaneous meshing of three gear pairs with same contact ratio, thus giving rise to 6–9 number of contact lines in the contact zone. The length of each contact line varies during meshing. This variation depends on base helix angle (α_b), transverse pitch (P_t), and the distance traveled by the contact line, which subsequently depends on any instant of time t from the start of the contact zone and the pitch line velocity (v). Fig. 2b illustrates the variation of a contact line in the contact zone for a single-gear pair shown in Fig. 2a. The term f_1 indicates the distance during which there will be no change in the contact line. The term f_2 implies the distance in which a contact line vanishes. The equation to calculate these two terms is given in Fig. 3. An algorithm is proposed to determine the variation in the length of contact lines [27] in the helical gear pair as illustrated in Fig. 3. The total contact lines for one transverse pitch travel of the pinion (P_t) is calculated by the summation of all the lengths of individual contact lines. This algorithm can be extended to determine the contact line variation for one rotation of the pinion by repeating it n number of times, where n is the number of teeth in the pinion. Furthermore, the algorithm can also facilitate in determining the contact line variation for defects like missing tooth (i.e. contact line).

This algorithm is applied to the 2nd gear pair of the gearbox for determining the length of the contact lines for one rotation of the 2nd main gear. Contact lines for $d0$, $d1$, and $d2$ defective conditions in that gear are compared and illustrated in Fig. 4a. Similarly the respective variation in length of the contact lines in the contact zone is illustrated in Fig. 4b. It can be observed that for two teeth missing i.e. $d2$ case, there is a contact

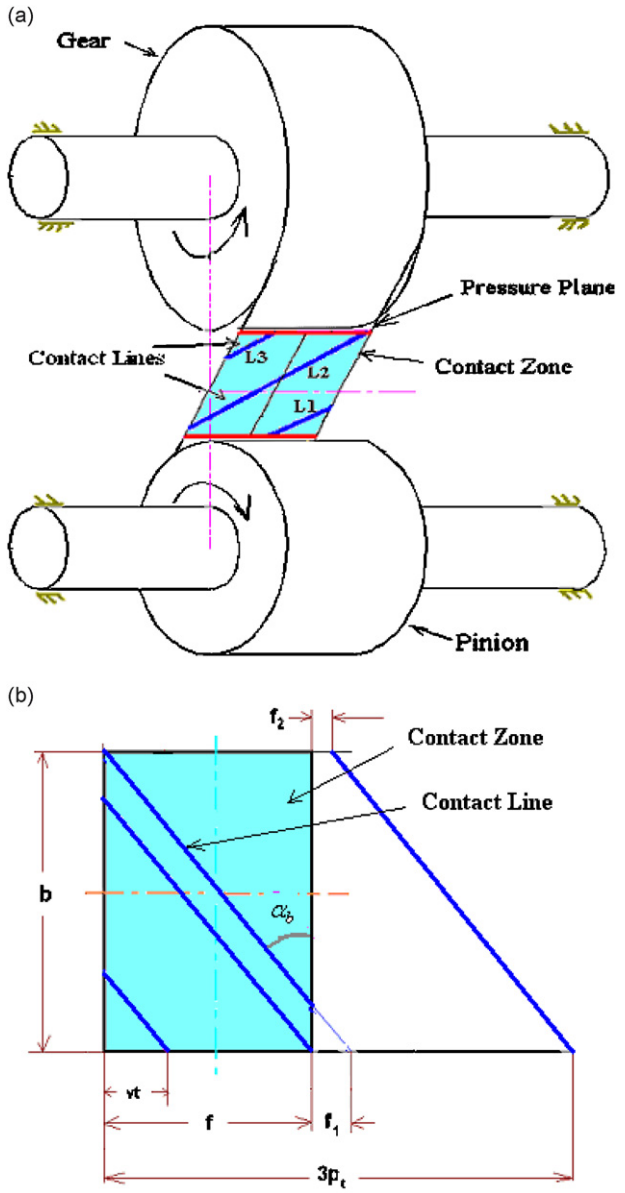

Fig. 2. (a) Contact zone of a single stage helical gear. (b) Variation of contact lines in the contact zone with various terminologies used.

loss for a very small duration as the contact ratio of the gear is 2.9. But because of synchro-meshed condition, defect-free 3rd and 4th gears will be responsible for continuous power transmission. Table 2 indicates the mean value of the length of contact lines in 4th, 3rd and various defective cases of 2nd gear for one rotation of each gear and for a travel of one contact zone. Table 3 shows the total mean length of contact lines for the defective cases considering all the gears are under synchro-meshed conditions. The percentage of contact loss is determined by applying Eq. (1):

$$\delta L^{di} = \frac{L^{d0} - L^{di}}{L^{d0}} \times 100, \tag{1}$$

where L^{d0} is the total length of contact lines in all the contact zones for defect-free case, L^{di} is the total length of contact lines in all the contact zones for ith defective case, δL^{di} is the percentage loss in contact lines for ith defective case for $i = 1$, 2, and 3.

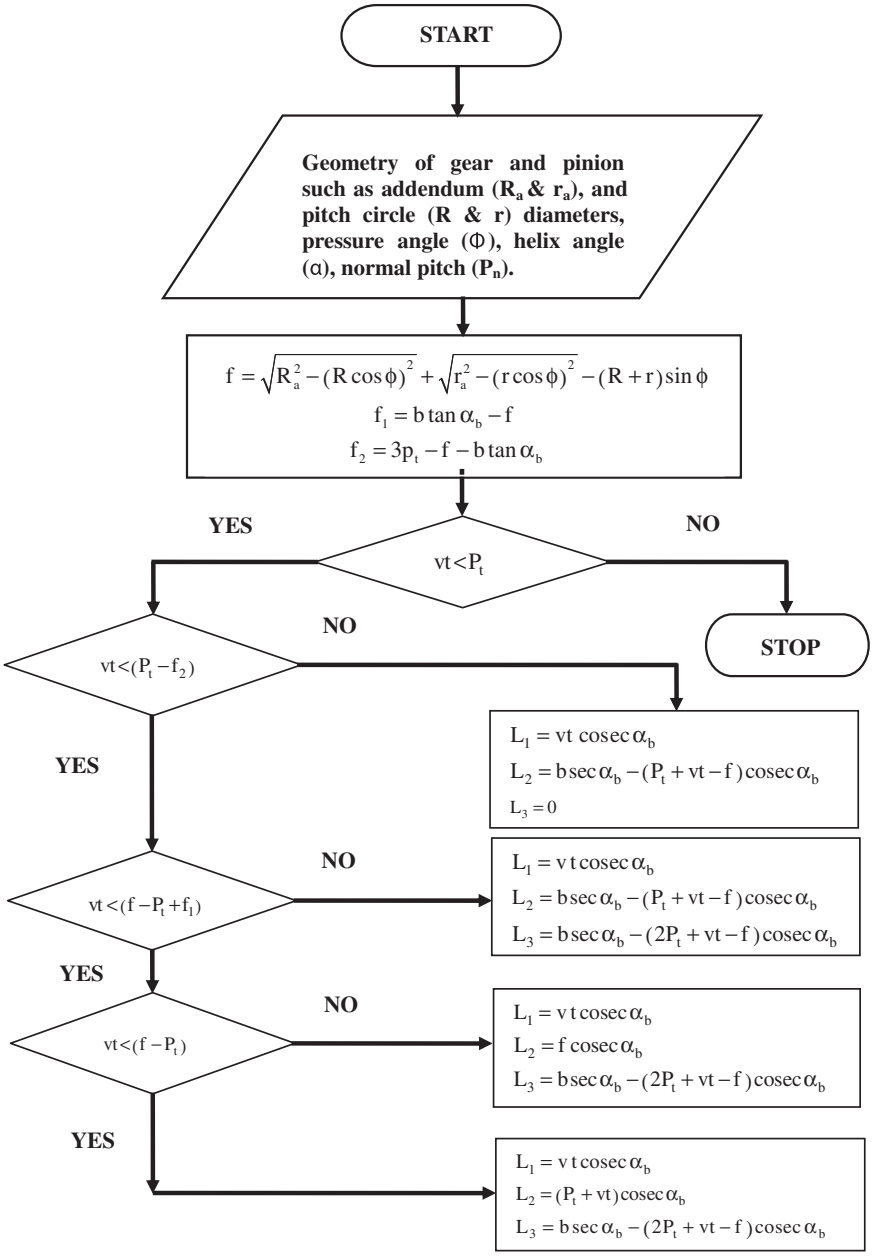

Fig. 3. An algorithm to determine contact line variation in helical gears with respect to time t.

It is observed that $d1$ defective case is equivalent to missing 1.15% of contact lines per one rotation of 2nd gear and 12.04% of contact lines in the contact zone. Similarly, for $d2$ defective case, the same will be 2.33% and 22.89% of contact loss, respectively. Contact loss for the $d3$ case will be the same as that for $d2$ condition. In real life, a helical gear can have a severe fault like four teeth broken in proportion [26].

2.2. Motor current signature analysis

Yacamini et al. [21] have observed from their simulation results that any shaft twisting torque will be reflected in the air gap torque of the induction motor, and the torsional vibration largely affects the torque-producing component of current, while magnetizing component has almost negligible effect on it. In Ref. [10],

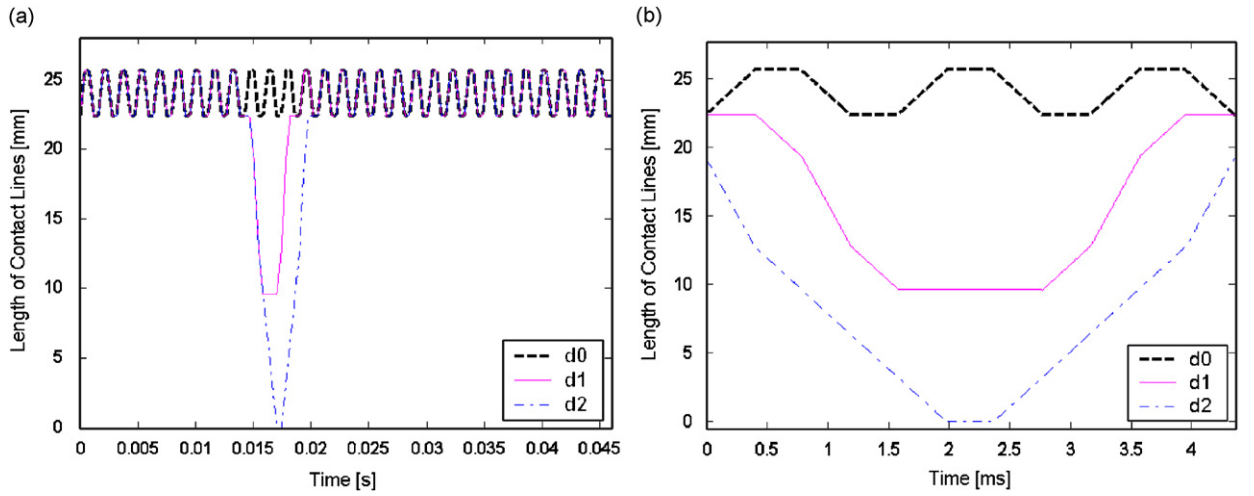

Fig. 4. Variation in length of contact lines of 2nd main gear for various defects in 2nd main gear: (a) in one rotation of the gear and (b) in the contact zone.

Table 2
Mean length of contact lines for various defect-free and defective gears

Gear	Defective case	Mean length of contact lines (mm)	
		One rotation	One contact zone
2nd main	Defect free ($d0$)	24.03	24.17
	One tooth missing ($d1$)	23.2	15.44
	Two teeth missing ($d2$)	22.37	7.57
2nd counter	Two teeth missing ($d3$)	22.37	7.57
3rd	Defect free	24.08	24.23
4th	Defect free	23.93	24.09

Table 3
Percentage contact loss due to various defective cases

Defective case	Total mean length of contact lines (mm)		% contact loss	
	One rotation	One contact zone	One rotation (%)	One contact zone (%)
$d0$	72.06	72.49	0	0
$d1$	71.23	63.76	1.15	12.04
$d2$	70.38	55.89	2.33	22.89
$d3$	70.38	55.89	2.33	22.89

the authors have also shown that defect induced in the gearbox will produce sidebands of its characteristic frequencies across supply line frequency in the induction motor expressed by the following equation:

$$I_s = I_0 \sin\left(2\pi f_e t + \phi_0\right) + \sum_{i=1}^{n}\left(\frac{A_{sT_i} + A_{sM_i}}{2}\right)\cos\left(2\pi\left(f_e - f_{ri}\right)t - \phi_i\right) + \sum_{i=1}^{n}\left(\frac{A_{sT_i} - A_{sM_i}}{2}\right), \times \cos\left(2\pi\left(f_e + f_{ri}\right)t + \phi_i\right), \quad (2)$$

where f_e is the supply line frequency, I_s the stator current of the induction motor, I_0 the average current drawn by the supply line frequency, A_{sT} and A_{sM} the torque-producing and magnetizing components of current,

respectively, f_i is the ith defect frequency with n-number of defect frequencies, and ϕ_0 and ϕ_i are the phase difference for f_e and f_i, respectively. These characteristics frequencies in a gearbox are the rotating shaft frequencies and GMF.

The effect of oscillating load, which is a sum of sinusoidal functions of various frequencies, on the current signature has already been discussed by Schoen and Habetler [24,28]. The electromagnetic torque, as expressed in Eq. (3), will have oscillations with the same frequencies as that of the load torque assuming a linear system:

$$T_e = \frac{3}{2}\frac{p}{2}(\lambda_{ds} i_{qs} - \lambda_{qs} i_{ds}), \tag{3}$$

where p is the number of pole; λ and i are the flux linkage and current, respectively, along quadrature (qs) and direct (ds) axes of stator. It is also observed that the fault conditions such as rotor eccentricity and the load torque will have the same low-frequency sidebands across supply line frequency given by Eq. (4), where f_e, f_{ecc} and f_{load} are supply line frequency, and frequencies due to rotor eccentricity and load torque, respectively; s corresponds to slip in the motor and m is any positive integer:

$$f_{\text{ecc}} = f_{\text{load}} = f_e\left[1 \pm m\left(\frac{1-s}{p/2}\right)\right]. \tag{4}$$

Therefore, the fault condition is overwhelmed by the load torque condition, thus making it difficult to diagnose rotor eccentricity in the presence of oscillating load torque. But the phenomena are different due to the fact that the oscillating load torque affects the current component along quadrature axis only, whereas the faults affect the current components in both direct and quadrature axis. It is inferred in Ref. [24] that load torque is damped at higher harmonics and hence faults such as broken rotor bar can be detected up to 4th harmonics of supply line frequency. In Ref. [28], effect of load is removed by subtracting the estimated stator current along direct axis by the actual current, by virtue of which only the effect of fault condition will be prominent in the resulting current signal.

This paper also investigates the current transients due to removal of load for detecting faults in gears. Figs. 5a and b illustrate the vibration transient and current transient due to removal of 5.625 kW load. It can be observed that in vibration transients, sudden removal of load will have instant change in the acceleration level, whereas the current transients takes some time to reach the steady state. Since GMF in the vibration signature are of the order of 630, 780, and 930 Hz [10], their detection in the current transient analysis is not possible applying the methods used in Ref. [28]. Therefore, advanced signal processing techniques like DWT and corrected MFT are applied to the current transients for the fault detection in the gears.

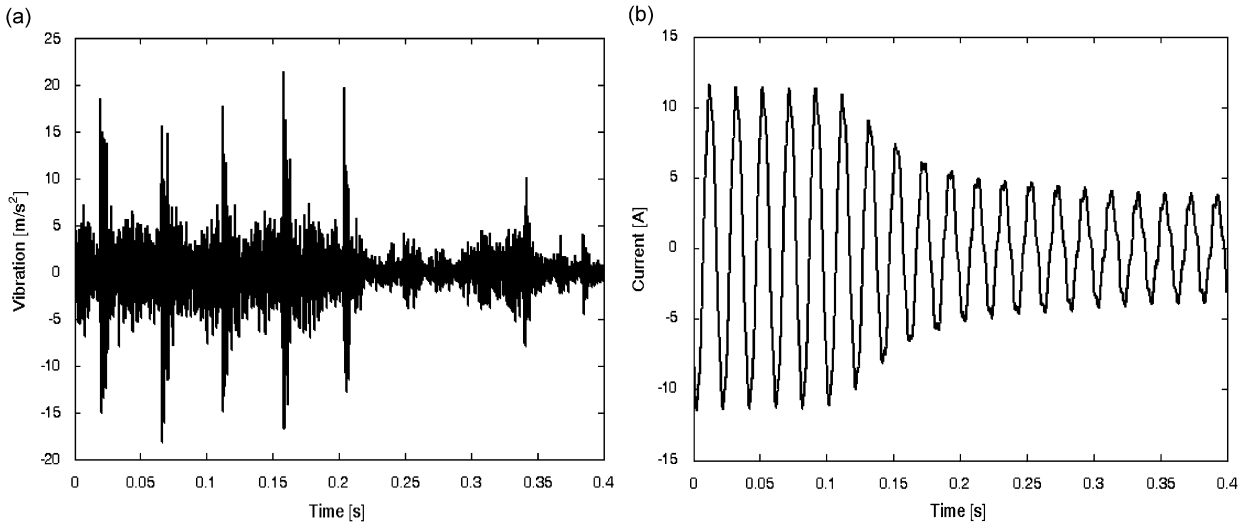

Fig. 5. Transients due to removal of 5.625 kW of load: (a) vibration transients and (b) current transients.

2.3. Discrete wavelet transform (DWT)

DWT can be classified into analysis and synthesis. Analysis involves decomposition of a signal into a low-frequency component known as approximate and a high-frequency component known as details. The approximate can again be decomposed into another approximate and details. The number of decomposition is known as levels. Synthesis reconstructs the original signal by adding the last level approximate and all details level. This decomposition can be carried out directly by using some defined orthogonal wavelets such as 'Daubechies', 'Haar', etc., where the convolving of scale and wavelet function of this wavelet with the signal will result in approximate and details, respectively. The scale and wavelet functions of a mother wavelet 'Daubechies 8' (or 'db8') used in this paper has already been shown in Ref. [10]. A DWT tree illustrated in Ref. [10] has also been used in this paper for analyzing current transients, which is a typical example of dyadic decomposition where the frequency for the next approximate is exactly divided by 2. The advantages of applying DWT are that the signal to noise ratio can be improved upon by separating high-frequency noise, and any details or approximate will be devoid of interference of the other levels.

2.4. Multiresolution Fourier transform (MFT)

MFT is a combination of both the STFT and WT. Unlike a wavelet used in WT, MFT uses a scaled window that convolves with the signal. The scaled window is shifted through out the scaled signal in order to get an equivalent STFT at that scaled signal. The advantage of such a technique over WT is that whereas WT can decompose a signal to different bandwidths, MFT maps the energy level of all the frequencies present in that frequency bandwidth. Eq. (5) is used to scale a window and Eq. (6) is used to find the MFT at a particular scale:

$$w_a(t) = \sqrt{a}w(ta), \tag{5}$$

$$\hat{x}(t,f,a) = \int_{-\infty}^{\infty} w_a(t-\tau)x(\tau)\,\mathrm{e}^{-\mathrm{i}2\pi f\tau}\,\mathrm{d}\tau, \tag{6}$$

where w_a denotes the window w at a scale a, τ denotes time translation and $\hat{x}$ denotes the MFT coefficients. Eq. (6) is very similar to STFT except that a scaled window is used in this equation. Eq. (5) implies that with increase in scale, the temporal resolution will be improved, but frequency resolution is impaired. The disadvantage of this technique is similar to that of CWT i.e. the infinite range of integration will produce a number of redundant scales and also will result in large computation time. Already the authors [10] have shown the inability of CWT to detect defects in a gearbox while investigating the motor current signals. Therefore, a corrected MFT is used by the authors in order to investigate vibration, and current signals under steady loads [23]. The scaling is carried out using DWT and then a hanning window is applied to the scaled signal. MFT will be equivalent to an FFT analysis if a single hanning window is used for the whole time record; and equivalent to STFT, if a number of windows are convolved with the signal having some overlapping. The temporal resolution depends on the width of the window and percentage of overlapping. In this paper, a hanning window of 256 data points is moved with 50% overlapping in the time record of vibration and current signals with 8192 number of data points. This will be equivalent to using 62 windows for the whole time record.

3. Experimental setup

Fig. 6a shows the experimental set-up used for investigating the vibration and current transients whereas Fig. 6b shows the instrumentation details required for acquiring vibration and current signals. A Hall effect sensor (Tektronix: A 622) is used to measure the phase current drawn by the induction motor driving the transmission gearbox. The advantage of using a Hall effect sensor over a current transformer is that it has a higher frequency range, thus suitable for high-frequency monitoring in current signature. A piezoelectric tri-axial accelerometer (B&K: 4321) with frequency bandwidth 0–20 kHz is mounted at the tail-end bearing of the gearbox. The gearbox, though has four numbers of stages, only three stages (2nd, 3rd, and 4th gears) are

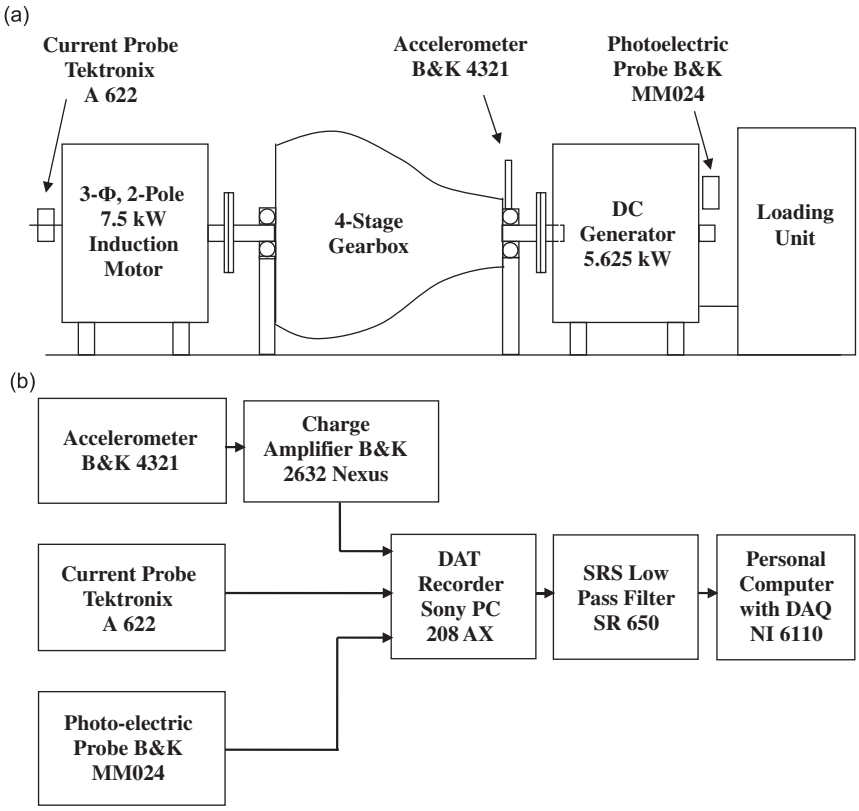

Fig. 6. (a) Experimental setup for the multistage gearbox. (b) Instrumentation details of the experimental setup.

synchro-meshed. Hence, at any operation of 2nd, 3rd, and 4th gear, all the three GMF will appear in the vibration signature. Similarly, there will be three rotating frequencies such as input, layshaft and output shaft frequencies In order to apply load, a separately excited DC generator is connected to the gearbox. The generator is electrically loaded through a resistance bank.

Effects of three artificially introduced defective cases $d1$, $d2$, and $d3$; discussed in Section 2.1 and Table 1 are covered in this paper. These defects are illustrated in Fig. 7. Fourteen number of load ranging from 375 to 5625 W have been removed to no load conditions and corresponding vibration and current transients are investigated. But, in this paper, three cases of transient loads such as 1.875 kW to 0 W, 3.75 kW to 0 W and 5.625 kW to 0 W are presented. Vibration and current transients with a maximum frequency of 10 kHz and 8192 number of data points are acquired into a personal computer using a 16-bit data acquisition card (NI PCI 6110) and LabView with a sampling frequency of 20.480 kHz and time record of 0.4 s. The signals are acquired in such a way that the load removal is centered at 0.2 s so as to focus attention at both loaded and unloaded region simultaneously. All the signals are analyzed in MatLab 6.5.

4. Results and discussions

4.1. Vibration transients

4.1.1. Discrete wavelet transform (DWT)

The authors have already established in Ref. [10] that in the steady vibration signature, all the rotating shafts and GMF appear. There are also sidebands of the rotating shaft frequencies and their harmonics across the GMFs. These rotating frequencies are input shaft frequency, layshaft frequency and output shaft frequency with an order of 49, 30, and 21 Hz, respectively. The GMFs are 2nd, 3rd, and 4th GMF with an

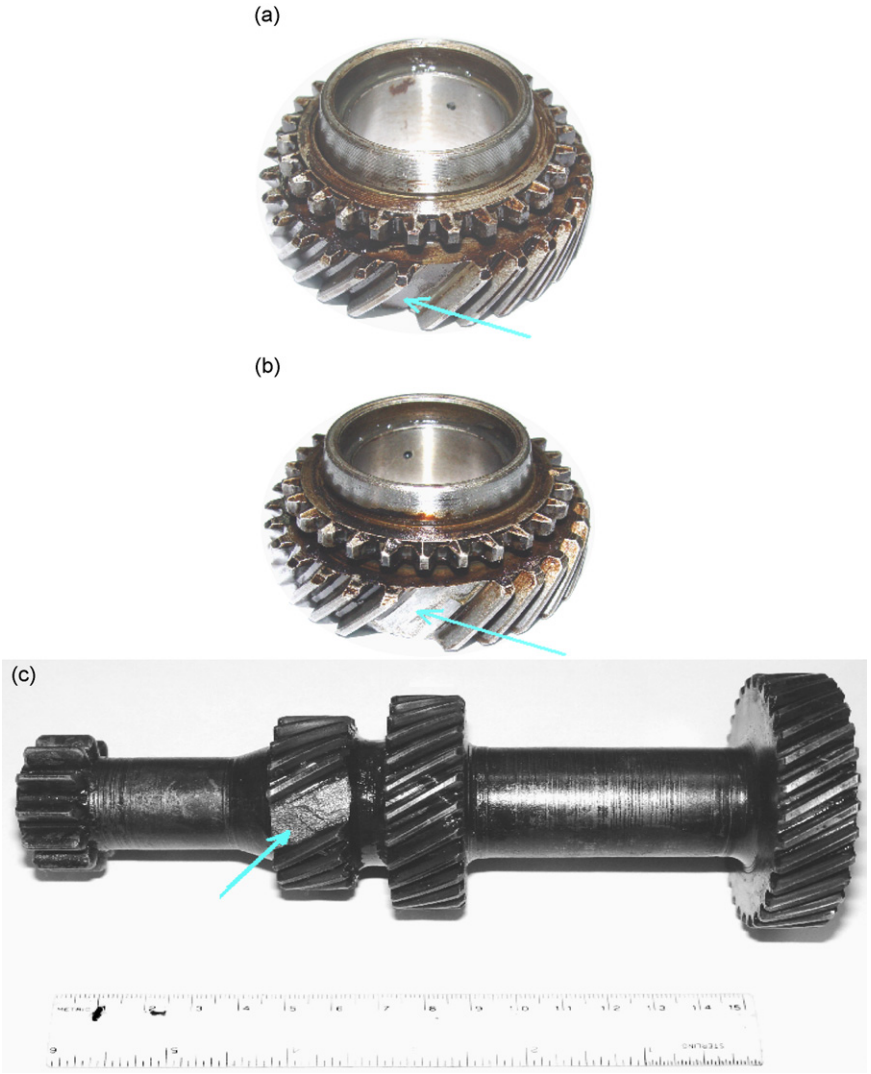

Fig. 7. Artificial defects introduced in different gears: (a) $d1$, (b) $d2$, and (c) $d3$.

order of 630, 780, and 930 Hz, respectively (Fig. 1). When the gearbox is operating at 2nd gear and there are defects in the 2nd gear, the 2nd GMF gains energy with increase in severity of defects.

Since, FFT analysis cannot be applied to vibration transients, as the sudden change in the acceleration level will induce spectral smearing, these transients are decomposed using DWT. The decomposition tree is illustrated in Fig. 13 of Ref. [10]. The details and approximate are termed as 'D' and 'A', respectively. The following number refers to the level of decomposition, e.g. D3 refers to details at 3rd level. Ten levels of decomposition have been carried out, where the D8 level has a frequency bandwidth of 39–78 Hz that contains information of output shaft frequency (of the order of 49 Hz). Similarly, D9 level can provide information of layshaft and input shaft frequencies. Out of the higher frequency levels, D4 level is the most important as all the GMFs lie in its frequency bandwidth of 0.625–1.25 kHz. D3 and other higher levels contain harmonics of the GMF. The levels to be focused will vary depending upon the rotating shaft frequency.

Fig. 8 illustrates the decomposed vibration transient with $d2$ defective condition at 5.625 kW transient load. The following observations are made:

1. D8 and D9 levels, and hence the rotating frequencies contribute very less vibration i.e. of the order of 0.1–0.2 m/s^2 in comparison to the transient, which has vibration severity of the order of 20 m/s^2. Moreover,

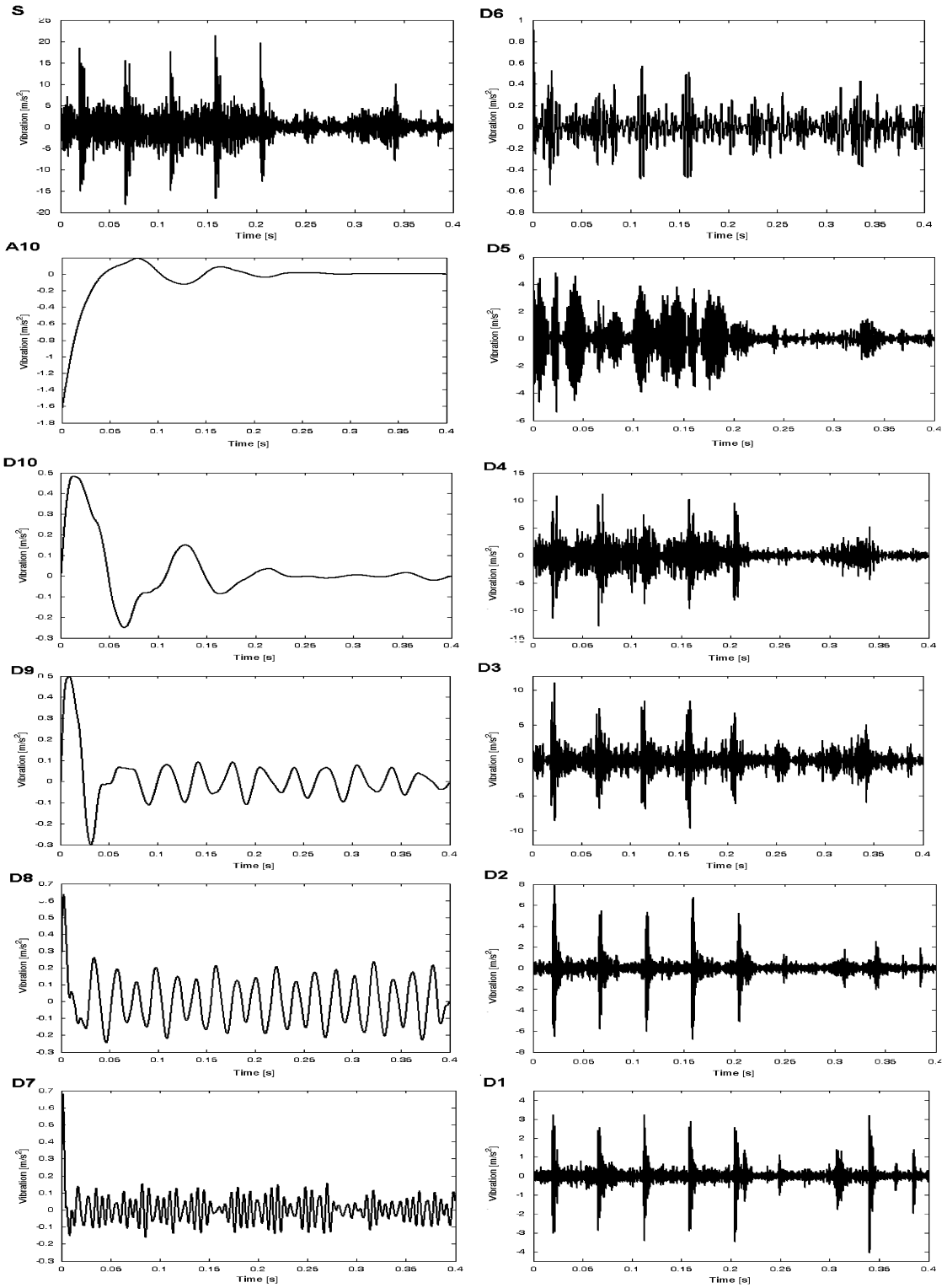

Fig. 8. Decomposition of vibration transient with $d2$ defect at transient load of 5.625 kW; from signal, approximate 10 and details 10–1.

these levels are negligibly affected by the transient load. This can be confirmed from the steady vibration signature analysis discussed in Ref. [10] that except for layshaft frequency, other rotating shaft frequencies do not undergo much change in amplitudes with change in steady load.

2. D4 level that contains the GMFs is the highest contributor to the overall vibration level with a $12\,m/s^2$ vibration level. It can also be noted that the change in amplitude levels due to transient load is highest in D4 level, from an acceleration level of $12\,m/s^2$ to an acceleration level of $2–3\,m/s^2$ at no load.
3. The next vibration severity level occurs at D3 level with amplitude of nearly $10\,m/s^2$.

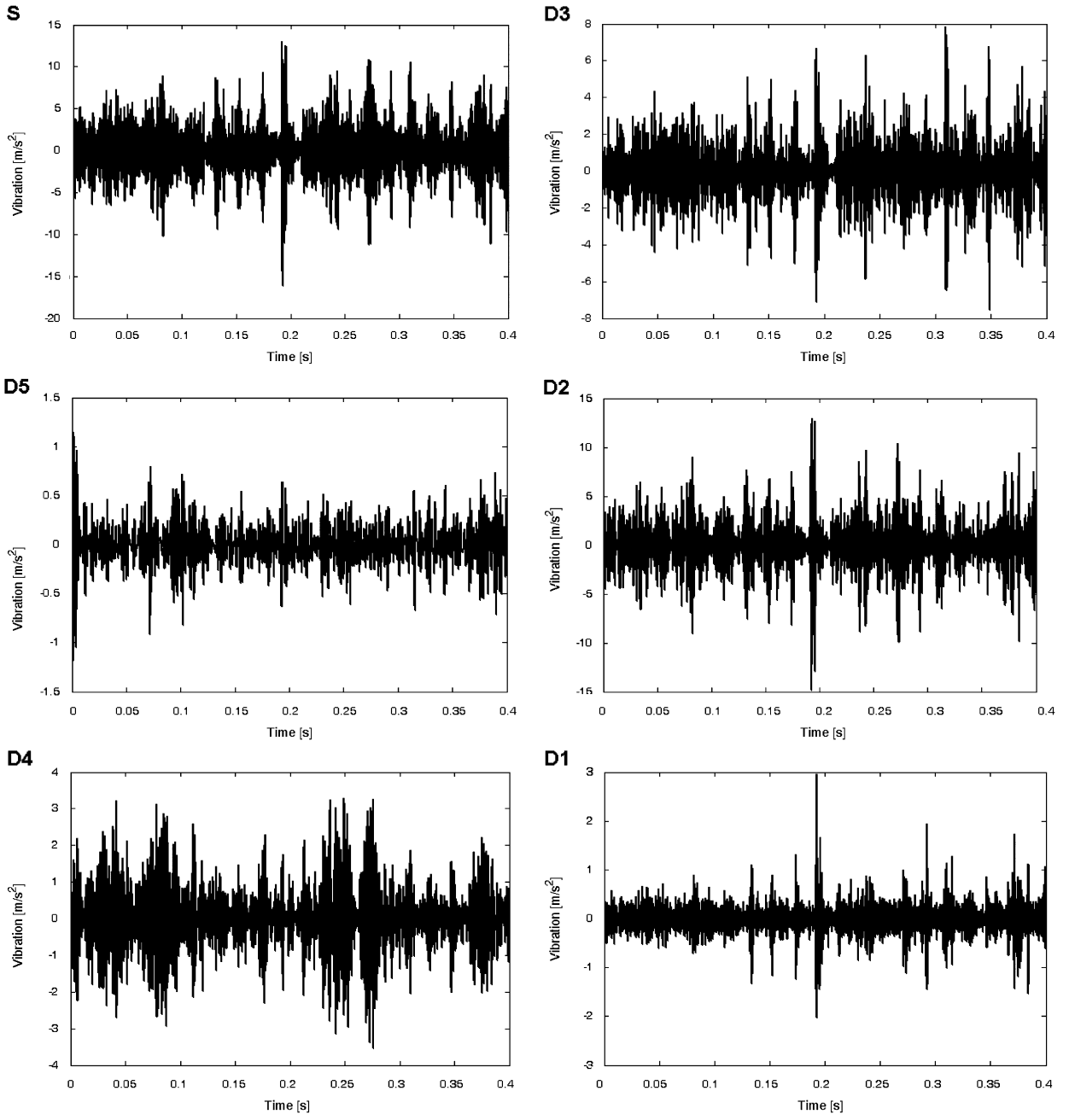

Fig. 9. Decomposition of vibration transient with $d0$ defect at transient load of 1.875 kW; from signal, details 5–1.

In all other defective cases and transient load conditions, same results are observed except for defect-free case ($d0$) and 1.875 kW transient load. A distinct phenomenon is observed for this case; illustrated in Fig. 9. The following observations are made:

1. The severity of vibration increases in the vibration transients at higher frequency level (D1–D4) after removal of 1.875 kW load. This implies that load acts as damping factor in case of defect-free gearbox and removal of load will increase the vibration level.
2. Vibration severity level of the signal is of the order of 15 m/s^2. Out of which, D2 level is the main contributor with a severity level of 14 m/s^2 in comparison to the vibration severity of 3.5 m/s^2 at D4 level. In all other defective and transient load cases, D4 level containing GMFs is most prominent contributors of vibration severity.
3. The load removal has negligible effect on rotating frequencies (D8 and D9 levels) as observed in other defective cases and hence not illustrated in Fig. 9.

These findings have been verified by plotting the DWT coefficients at 5.625 kW transient load condition as illustrated in Fig. 10. It is observed that there is a large impact after load removal for defect-free and 5.625 kW transient load condition (Fig. 10a). This validates the statement that load acts as damping factor for defect-free condition. Another important observation; which has also been inferred by Ball et al. [1,2] and Stander et al. [3]; is that with increase in severity of defects, the energy smears into other frequency regions.

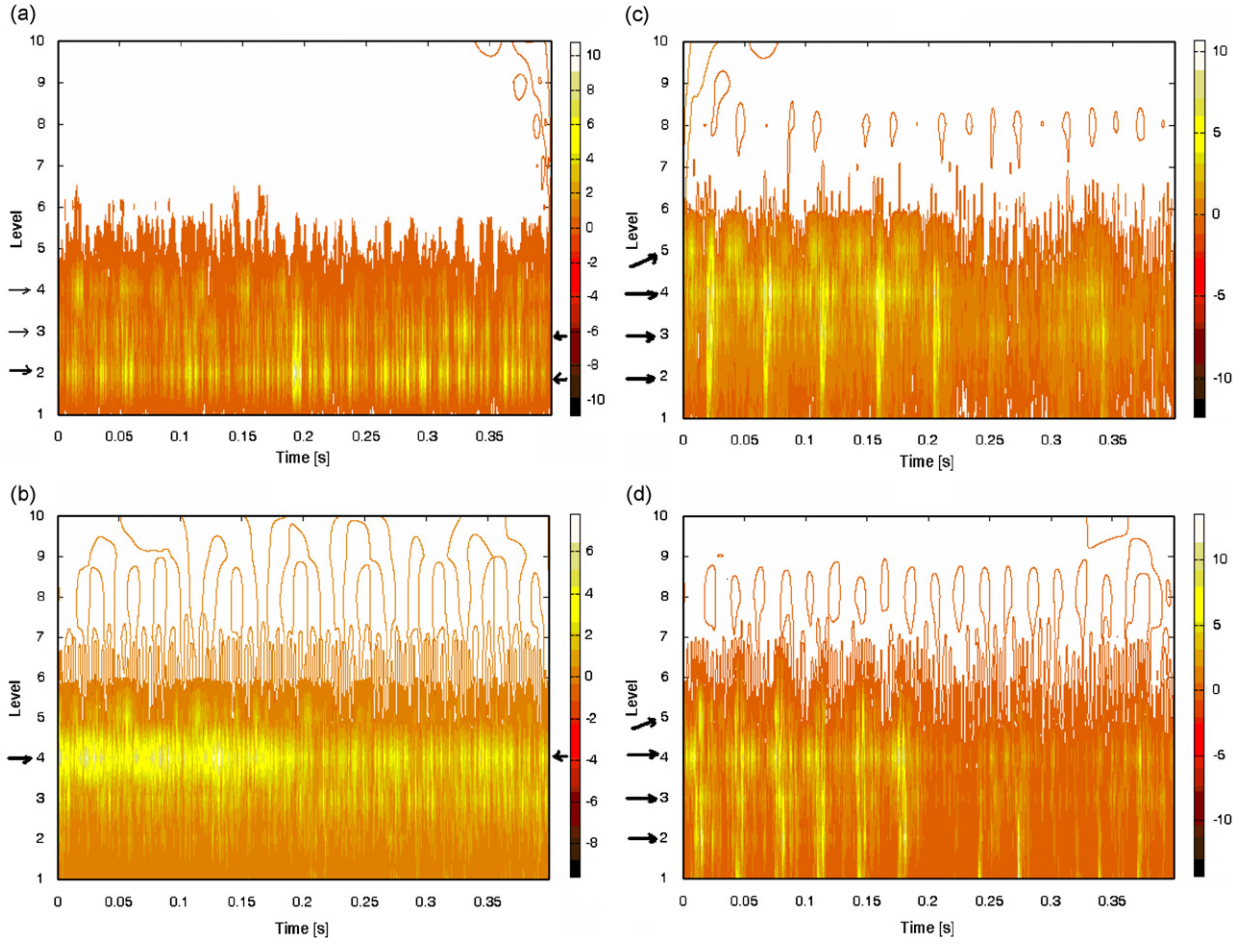

Fig. 10. DWT coefficients' plot of vibration transients at 5.625 kW transient load and following defective conditions: (a) $d0$, (b) $d1$, (c) $d2$, and (d) $d3$.

For example, for d1 defective case and 5.625 kW transient load, only D4 level contains the impact energy (Fig. 10b). But for *d*2 and *d*3 defective cases shown in Figs. 10c and d, the impact energy is distributed from D2 to D5 levels. Hence, it can be inferred that any vibration transients with a particular defective case and transient load has a specific probability distribution of its amplitudes [11].

4.1.2. *Multiresolution Fourier transform (MFT)*

The above section led to the inference that D4 level that contains all the GMFs is the important level where attention should be focused for more analysis. Therefore, corrected MFT described in Section 2.4 is applied to this level. A constant window MFT or equivalent FFT analysis will not give proper result as this level is largely affected due to transient load. Therefore moving window MFT or equivalent STFT analysis is applied to the D4 levels of vibration transients at all defective cases and transient loads. The result at 5.625 kW transient load is illustrated in Fig. 11. The following observations are made:

1. In defect-free case and at all transient loads (Fig. 11a at 5.625 kW transient load), the main energy carrier is 4th GMF (of the order of 930 Hz). There is no trace of 2nd and 3rd GMFs, even though the gear operates at 2nd gear. This is due to the fact that 4th gear is connected to the induction motor, as illustrated in Fig. 1, and mainly responsible for power transmission in any gear operation. For example, 4th and 2nd gears transmit power while 3rd gear rotates freely during 2nd gear operation.
2. With increase in severity of defect in the 2nd gear, the 2nd GMF (of the order of 630 Hz) gains energy.

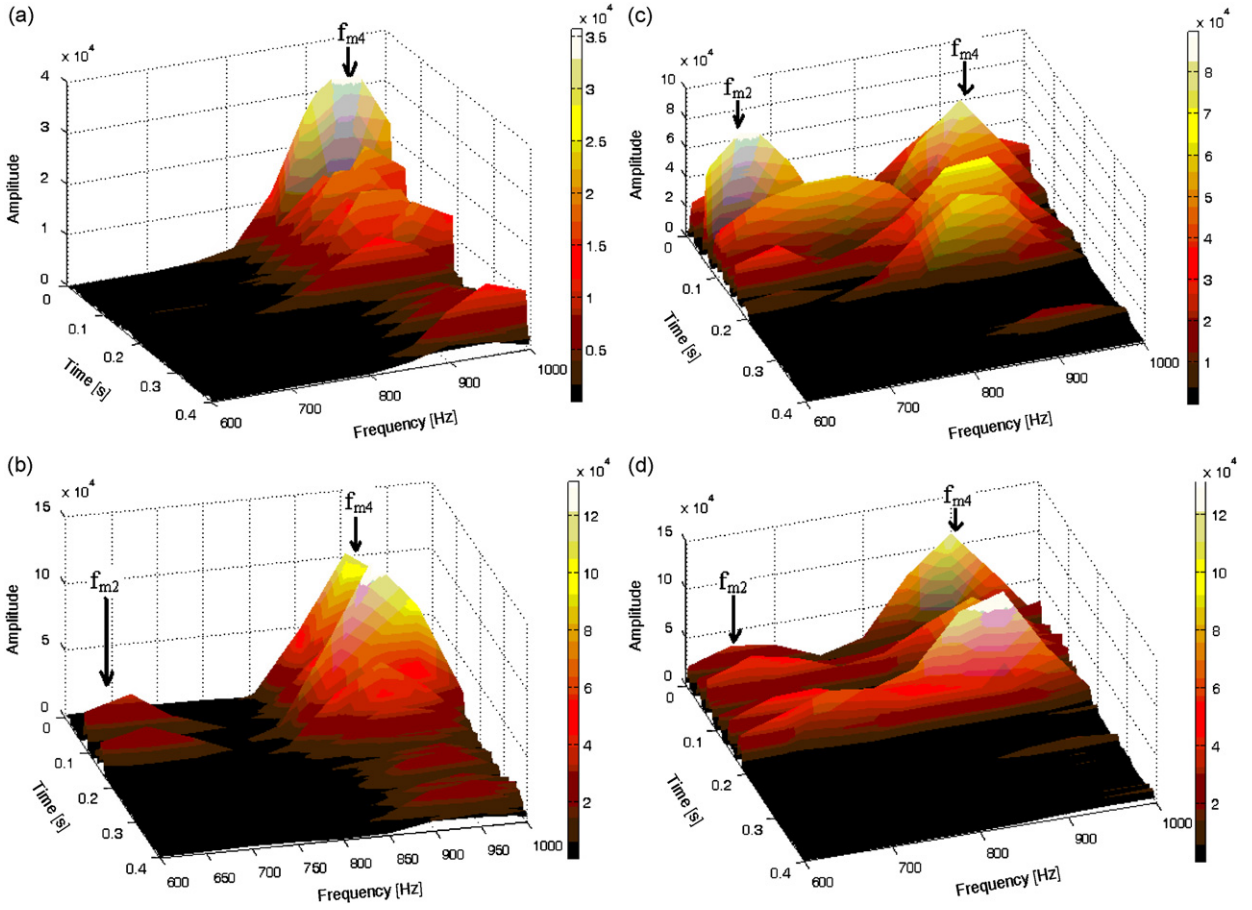

Fig. 11. MFT of vibration transients for details 4 level at 5.625 kW transient load and following defective conditions: (a) *d*0, (b) *d*1, (c) *d*2, and (d) *d*3.

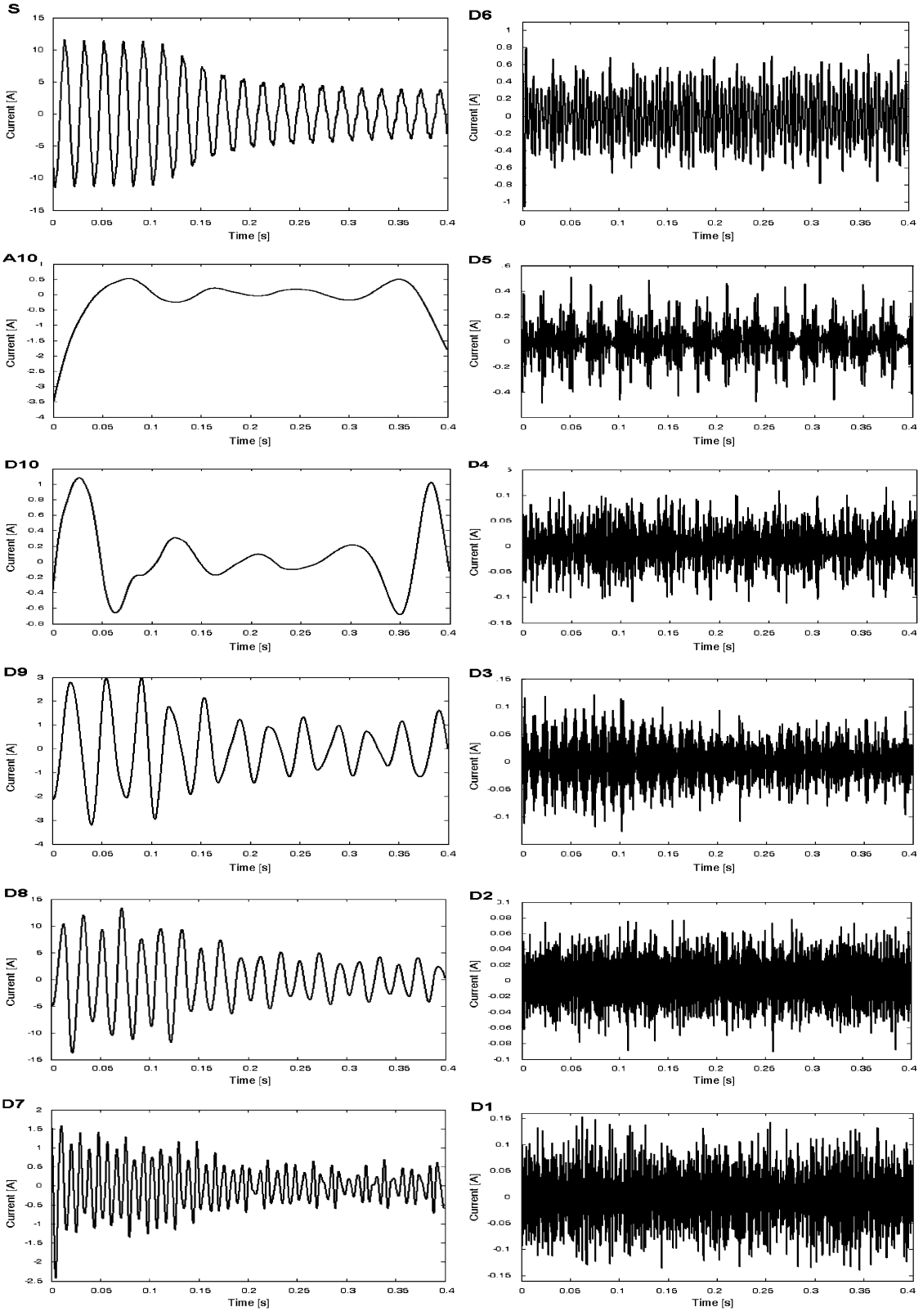

Fig. 12. Decomposition of current transient with d2 defect at load fluctuation of 5.625 kW; from signal, approximate 10 and details 10–1.

3. Fig. 11a again validates the point that for defect-free condition, vibration increases with removal of load. This effect is not observed for defective cases.

Hence, it can be inferred that MFT with moving window technique can map the impact energy due to defects in the vibration transients and hence can identify the types of defect.

4.2. Current transients

4.2.1. Discrete wavelet transform (DWT)

Current signatures at steady loads will have sidebands of the rotating shaft frequencies and GMF across supply line frequency [10]. Hence, D4 level with a frequency bandwidth of 625–1250 Hz will contain most of the sidebands of GMFs across supply line frequency. D3 level also contains the harmonics of the frequencies observed in D4 level. Since, the supply line frequency of 50 Hz has very high amplitude [10], D8 level with a frequency bandwidth of 39–78 Hz will be another important level to focus. The decompositions for current transients are carried out as per the same DWT tree illustrated in Fig. 13 of Ref. [10]. Fig. 12 illustrates the current transient, its 10th level approximate and from 10th level details to 1st level details at 5.625 kW transient load. The following observations are made:

1. Current transient has an amplitude of the order of 12–13 A, whereas 4th level details (D4) has an amplitude of the order of 0.12 A. But the details at 8th level (D8) has an amplitude nearly same as that of the transient.

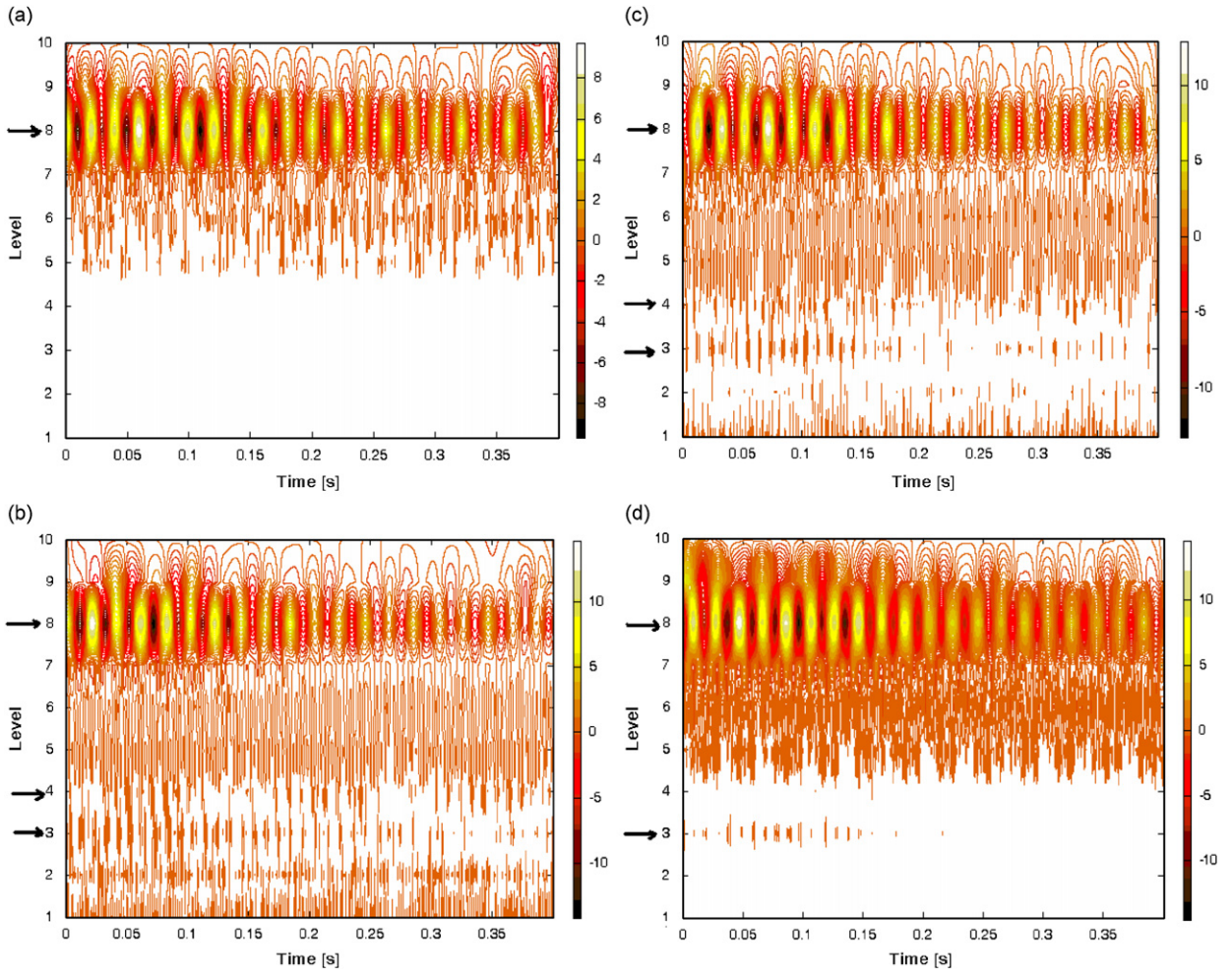

Fig. 13. DWT coefficients' plots of current transients at 5.625 kW transient load for following defect conditions: (a) $d0$, (b) $d1$, (c) $d2$, and (d) $d3$.

Therefore, it can be inferred that D8 level dominates the signal of D4 level and hence conventional FFT analysis will be inadequate in detecting the sidebands of the GMFs across supply line frequency.

2. Even the 1st level details (D1), which may contain high-frequency noise has an amplitude of the order of 0.12 A, thus making it difficult to trace the sidebands of GMFs.
3. Transient loads affect D7, D8, and D9 levels the most. D7 level contains the 2nd harmonics of supply line frequency, whereas D9 level contains the sidebands of output shaft and layshaft frequencies across supply line frequency. There is very little effect of removal of load on D4 level.

To observe the combined effects of transient loads and defects, plots of DWT coefficients of the current transients for all defective cases at 5.625 kW transient load are illustrated in Fig. 13. Current transients at other transient loads are not shown as these are equivalent to the case of no defect at 5.625 kW transient load (Fig. 13a). It is inferred that the transient loads affect D8 level the most. But for defective gears at 5.625 kW transient load, there is a very low energy transient at D4 and D3 levels. Fifty contours have been drawn in order to enhance the energy resolution to highlight this region, as the amplitude of current drawn is of the order of 0.15 A in the above levels, in comparison to that of 14 A in D8 level (Fig. 12).

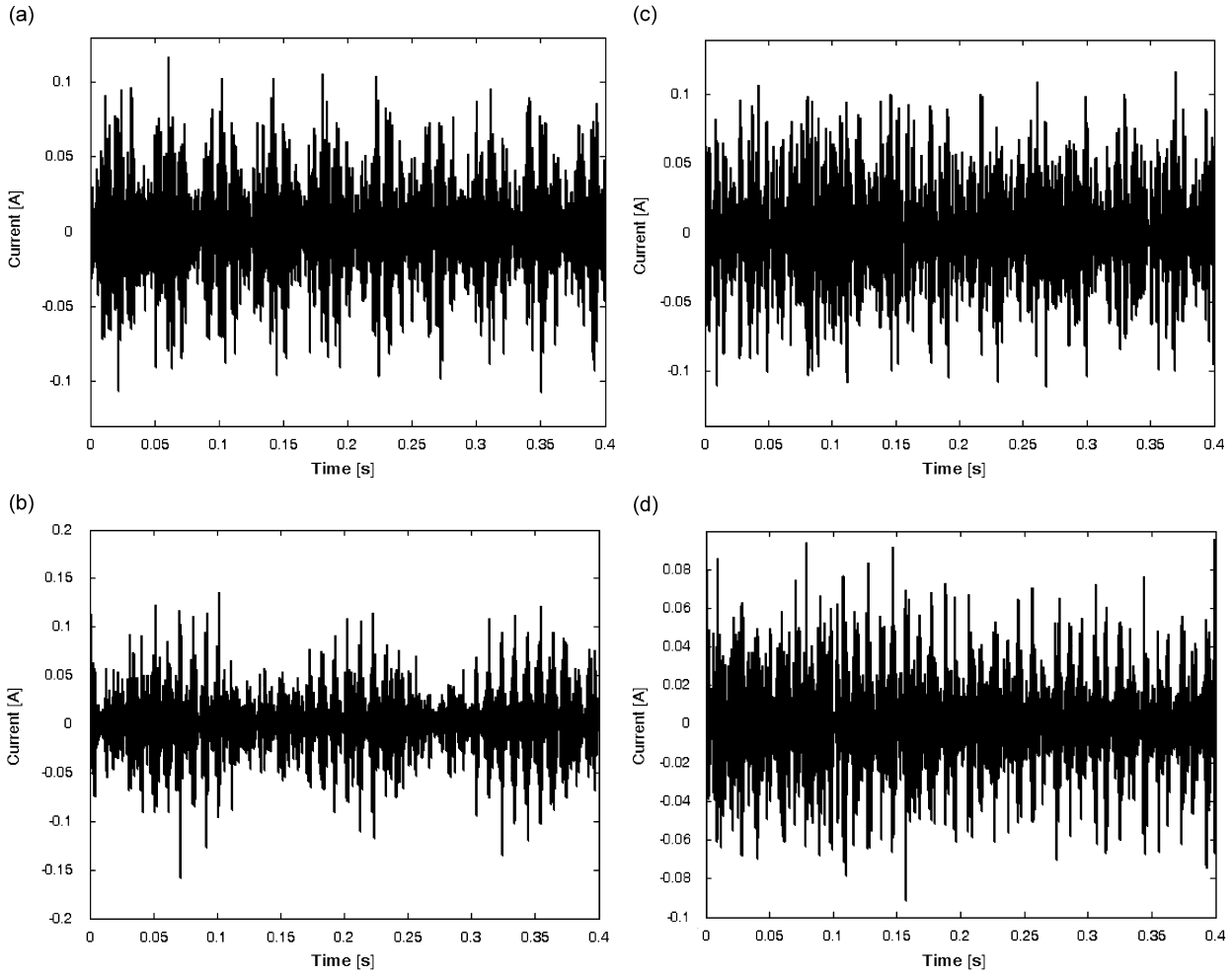

Fig. 14. Time-domain representation of D4 level of current transients at 5.625 kW transient load and for following defect conditions: (a) *d*0, (b) *d*1, (c) *d*2, and (d) *d*3.

4.2.2. Multiresolution Fourier transform (MFT)

4.2.2.1. Constant window MFT (equivalent FFT analysis). Since the effect of the transient load is very less in the D4 level of current transients, FFT analysis is carried out by convolving with it a hanning window for the whole time record. Fig. 14 shows the time domain current transient at 4th level details and their FFT analysis is illustrated in Fig. 15 at 5.625 kW transient load. Following observations are made from this analysis:

1. The technique is effective enough to monitor even a small amplitude of 1 mA.
2. It can be observed from the time series of D4 levels (Figs. 14a–d) that the amplitude levels for all defects is nearly same with an order of 0.12 A. But their frequency domain representations (Fig. 15) vary widely with severity of defect. Fig. 15a has a dominant 13th harmonics of supply line frequency, of the order of 14 mA. But with increase in defect severity, its energy is distributed to the sidebands of GMFs across supply line frequency. The same inference had been drawn in Ref. [10].
3. The time series of D4 level of current transient for d1 defect case (Fig. 14b), contains large transients and hence spectral smearing in its FFT (Fig. 15b) is very difficult to be interpreted.
4. Since, the lower limit of the bandwidth is 625 Hz, hence a large energy is concentrated near 630 Hz which is equivalent to the input shaft sideband of 2nd gear mesh frequency across supply line frequency ($f_{m2}+f_1-f_e$).

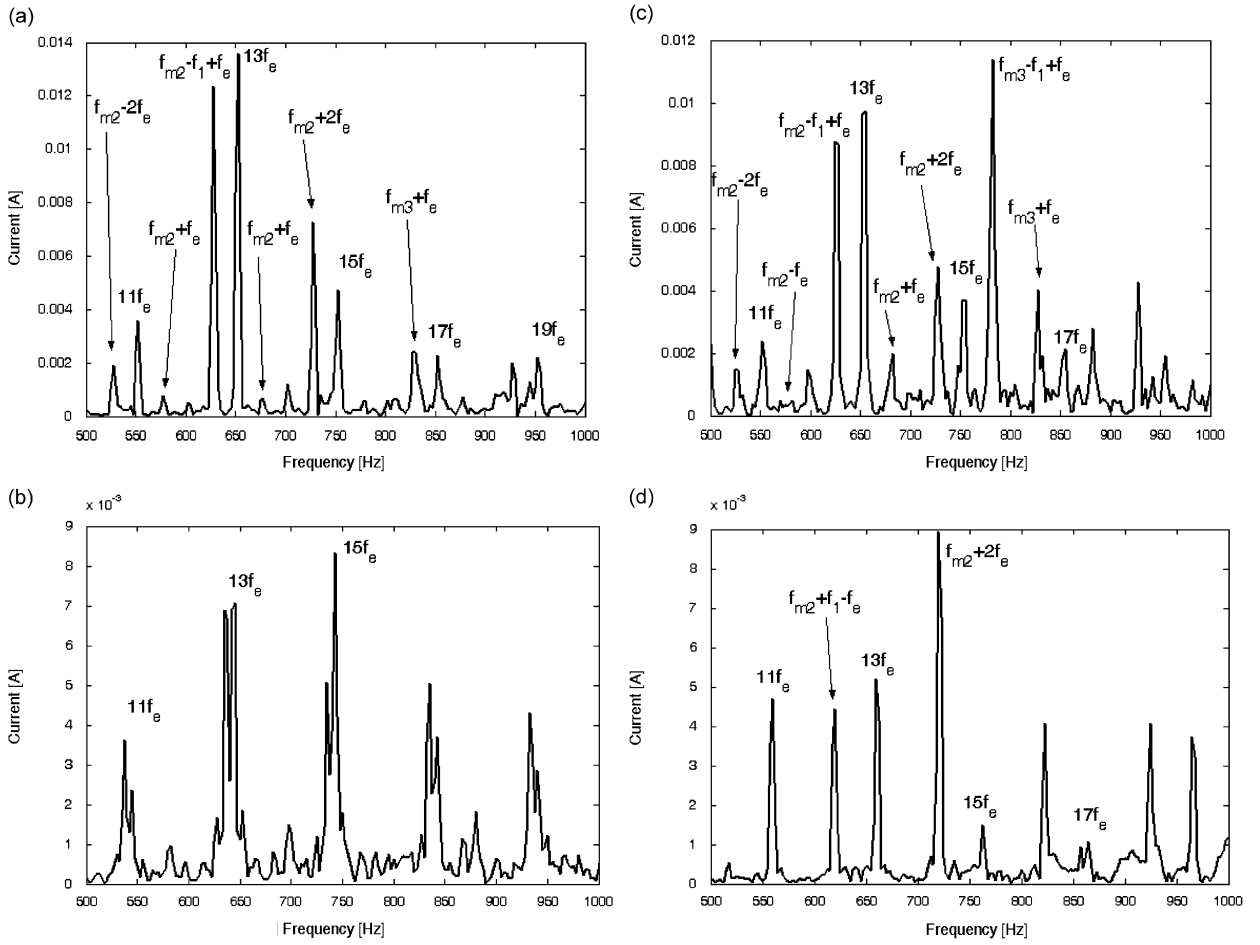

Fig. 15. Frequency domain representation of D4 level of current transients at 5.625 kW transient load and for following defect conditions: (a) *d*0, (b) *d*1, (c) *d*2, and (d) *d*3.

4.2.2.2. Moving window MFT (equivalent STFT analysis). To determine equivalent STFT analysis, 62 number of hanning windows with 50% overlapping are convolved with D4 levels of all defective and transient load cases. The equivalent STFT coefficients at 5.625 kW transient load are plotted in Fig. 16. The following observations are made:

1. For defect-free case (Fig. 16a), the dominant feature is found to be 650 Hz ($13f_e$). But with increase in defect severity, energy is excited in the higher frequency region by the transient loads.
2. It is very easy to classify defects at very high transient loads (5.625 kW) as the energy spreads to the sidebands. Moreover, the higher frequency regions are excited with increase in defect.
3. The effect of transient load is not much at D4 levels of the current transient.

The effectiveness of this technique in comparison to the technique described by Schoen and Habetler [24,28] is as follows:

1. This technique could separate out the effect of load from the effect of defects in the current transients due to transient loads.
2. Defect frequencies higher than 4th harmonics and up to 20th harmonics of supply line frequency could be detected.

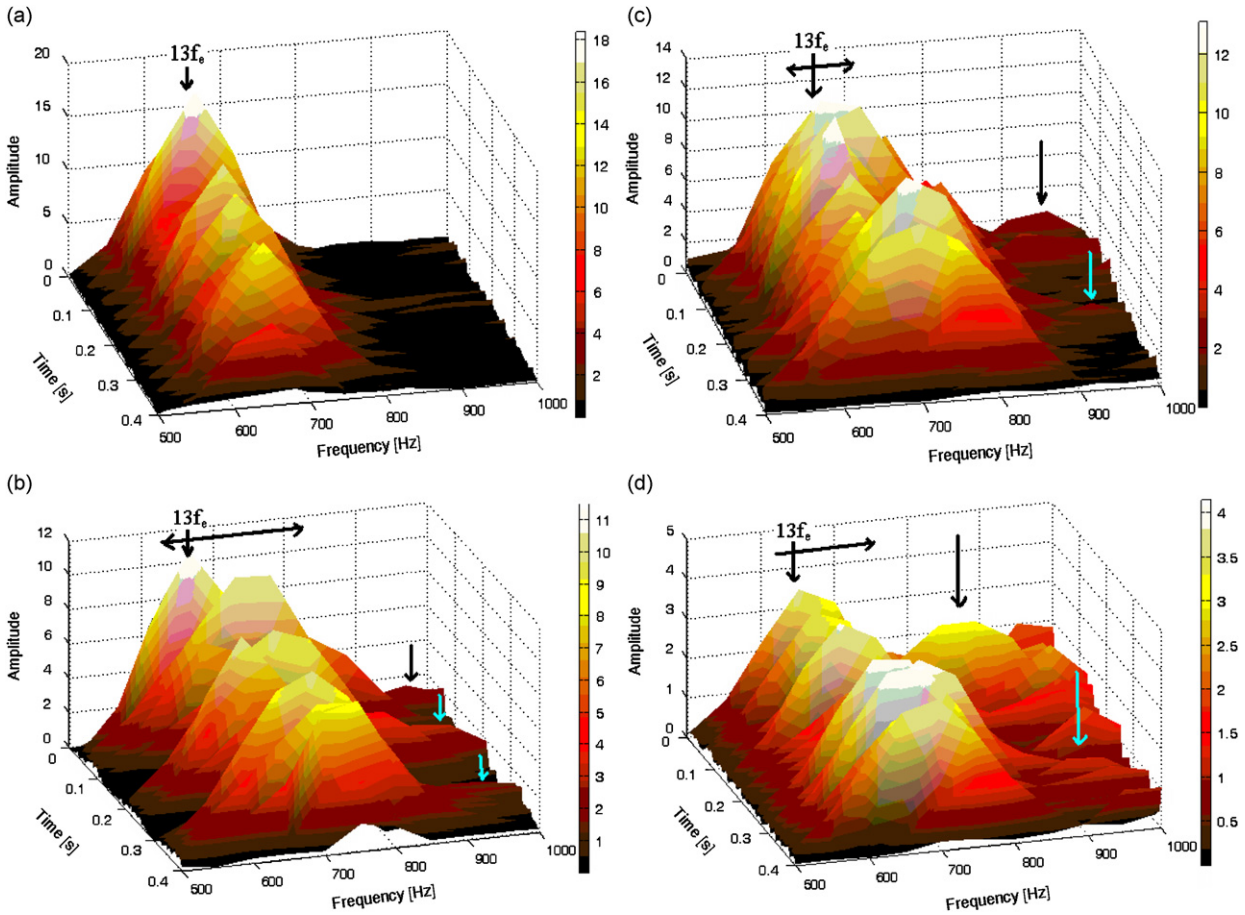

Fig. 16. MFT of current transients for details 4 level at 5.625 kW transient load and following defect conditions: (a) $d0$, (b) $d1$, (c) $d2$, and (d) $d3$.

4.3. Feature extraction from MFT coefficients

Figs. 11 and 16 depict qualitative analysis of vibration and current transients, where a change in the values of MFT coefficients with frequency is observed. A statistical feature extraction technique is employed in order to quantify the severity of defect, which is described below:

1. The 500–1000 Hz bandwidth of D4 details level of each transient is divided into 11 frequencies beginning from 500 Hz with 50 Hz increments.
2. The rms value of the MFT coefficients is determined for the whole time records all these frequencies, which indicate the energy content of any signal at a particular frequency.

Such a technique will have the following advantages:

1. The statistical techniques provides erroneous results when applied to signals with poor signal to noise ratio [11]. But the decomposed D4 level is devoid of high-frequency noise [10], and hence statistical techniques can be effective in pattern recognition in various signals.
2. The feature extraction technique can be used as an algorithm in order to computerize the decision-making process on defect severity.

The feature extraction technique is applied to the vibration and current transient at all the defective and transient load conditions.

4.3.1. Vibration transient analysis

The variation in the rms values of the MFT coefficient of vibration transient at various discrete frequencies has been summarized as in Fig. 17. It is observed from the figure that tracking of amplitude of any frequency

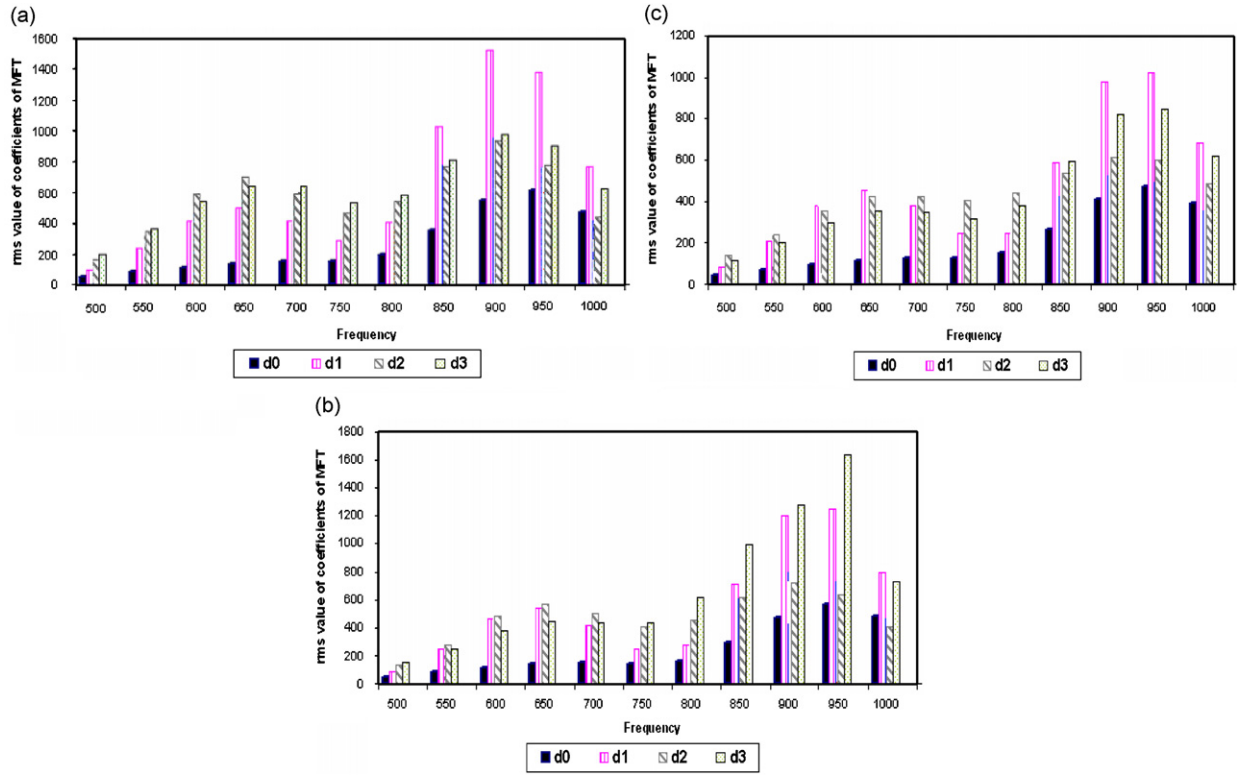

Fig. 17. The variation in rms value of the MFT coefficients of vibration transients at some discrete frequencies for following load transients: (a) 5.625 kW, (b) 3.75 kW, and (c) 1.875 kW.

within 900 Hz can detect defects. The trend at large transient such as 5.625 kW load removal (Fig. 17a) and below 800 Hz is $d3/d2 > d1 > d0$. But in case of large transients (5.625 kW) and above 850 Hz, and very small transients such as 1.875 kW load removal and 600–650 Hz, the trend is $d1 > d2 > d3 > d0$, which imply that defects can be detected at the earliest.

4.3.2. Current transient analysis

The summary of the variation in rms values of MFT of the current transients is illustrated in Fig. 18. It can be observed that defects like d1 and d2 can be detected at discrete frequencies above 750 Hz at 5.625 kW transient load (Fig. 18a). At 3.75 kW transient load condition (Fig. 18b), the frequencies above 900 Hz can be focused whereas for 1.875 kW transient load, there is a consistent decrease in the rms value of MFT coefficients at 600 and 650 Hz with a trend of $d0 > d1 > d2 > d3$. But $d3$ defect, i.e. two teeth missing in 2nd counter gear is difficult to be detected in the current transients.

5. Summary

Summary of the techniques used and inferences drawn are shown in Fig. 19. In case of vibration transients, GMFs are affected the most by the introduction of loads and defects in the gears (2nd gear). With increase in severity of defects, energy smears into low-frequency bandwidths. For defect-free case, the load removal increases the vibration level indicating that load acts as a damping factor. For current transients, though supply line frequency is the principal energy carrier, a low energy transient appear in the high-frequency region for defective cases. Use of MFT facilitated in highlighting this high-frequency region where the sidebands of the GMF across the supply line frequency lie. It is observed that for defect-free case, 13th harmonics of supply

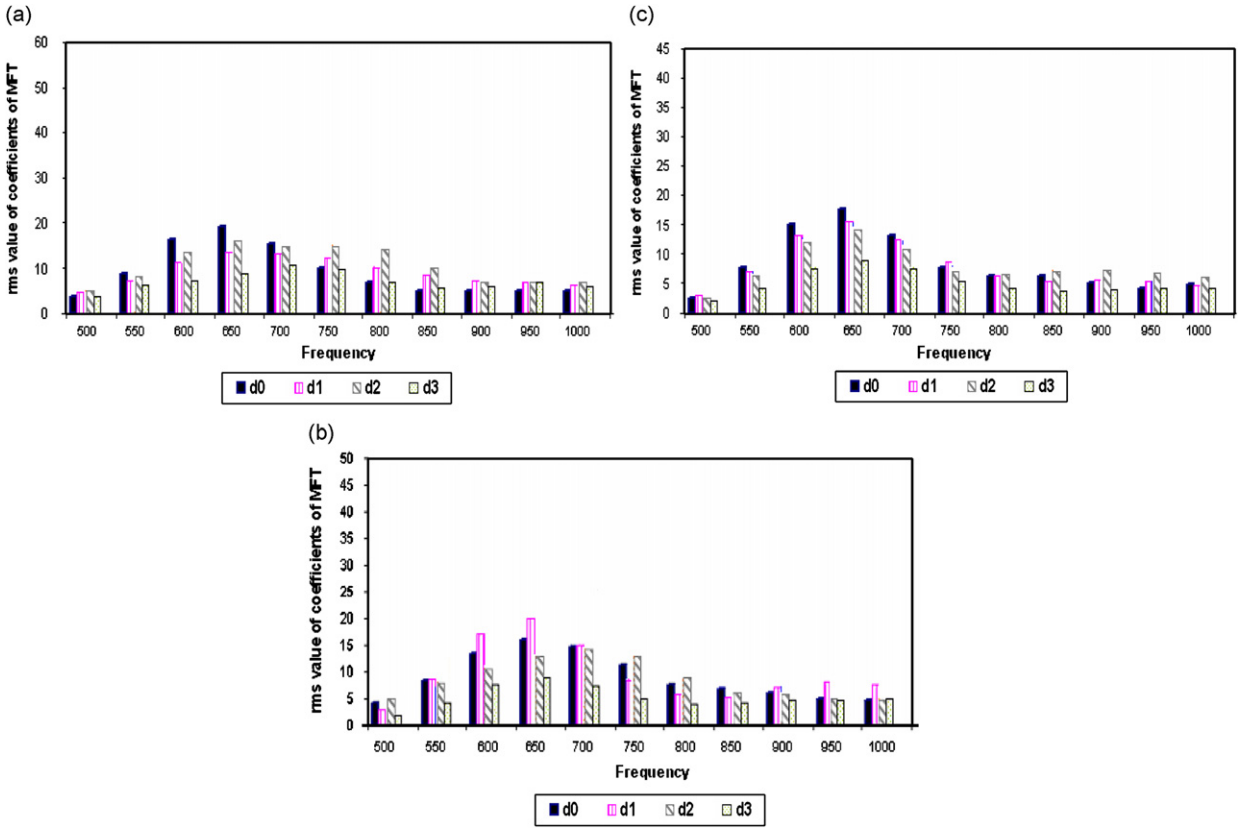

Fig. 18. The variation in rms value of the MFT coefficients of current transients at some discrete frequencies for following load transients: (a) 5.625 kW, (b) 3.75 kW, and (c) 1.875 kW.

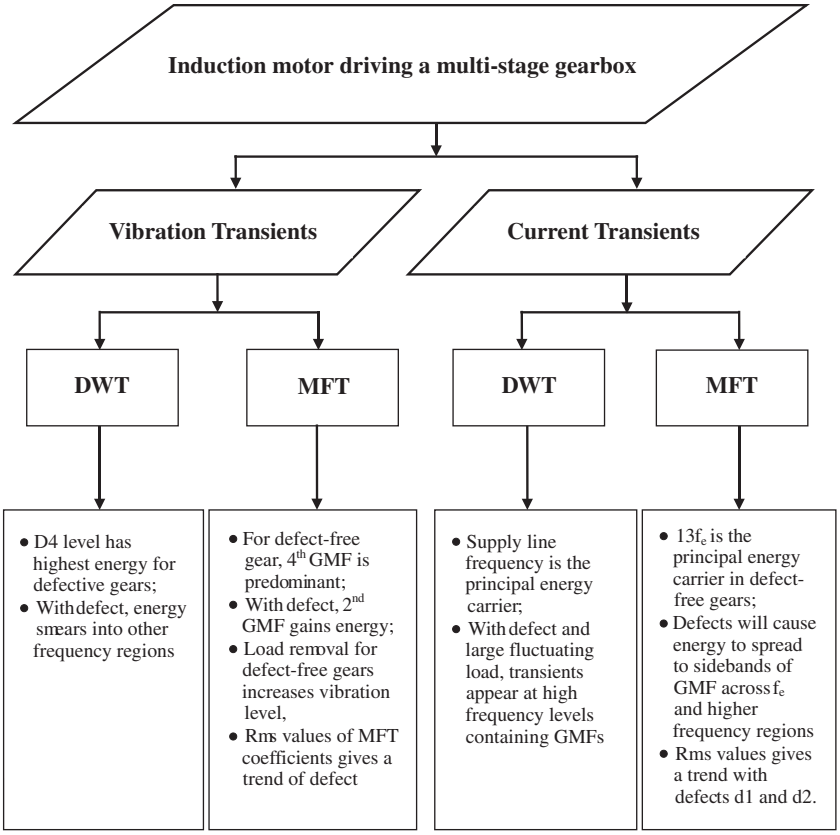

Fig. 19. Diagnostics decision flow chart in analyzing of vibration and current transients for gearbox fault detection.

line frequency was very dominant in D4 level. But with increase in defect, energy smears to the GMF sidebands of supply line frequency as well to higher frequencies, thus facilitating diagnosis of faults in gears. A statistical feature extraction technique is established by determining the rms values at discrete frequencies of the MFT coefficients of vibration and current transients. This methodology facilitates in finding a trend in the rms values depending on the defect severity, thus providing a pattern recognition technique.

6. Conclusion

The objective of this paper was to find a fault-monitoring scheme that can be applied to both vibration and current signals at transient load conditions. Vibration transient is a high-frequency phenomenon with dominating GMF, whereas current transient is a low-frequency phenomenon with dominating supply line frequency. Limitations of the time–frequency techniques such as STFT is that it will require two different window sizes for proper frequency resolution. Similarly, recently developed order tracking techniques can be very useful in monitoring only the vibration transients, where most of the frequencies are orders of the shaft speed. But, these cannot be applied to current transients, where the frequencies observed in the vibration signatures induce sidebands across supply line frequency. Hence, a corrected MFT is applied to both vibration and current transients, which maps the energy level of different frequencies at a particular frequency bandwidth, in order to distinguish various faults in gears undergoing fluctuation in loads. A monitoring scheme is developed for the transmission gearbox that can be the basis of future extension of this research on other variety of gears found in industries.

References

[1] C.J. Stander, P.S. Heyns, W. Schoombie, Using vibration monitoring for local fault detection on gears operating under transient load conditions, *Mechanical Systems and Signal Processing* 16 (6) (2002) 1005–1024.

[2] C.J. Stander, P.S. Heyns, Instantaneous angular speed monitoring of gearboxes under non-cyclic stationary load conditions, *Mechanical Systems and Signal Processing* 19 (4) (2005) 817–835.
[3] N. Byder, A. Ball, Detection of gear deterioration under varying load conditions by using the instantaneous power spectrum, *Mechanical Systems and Signal Processing* 14 (6) (2000) 907–921.
[4] F. Bonnardot, M.E. Badaoui, R.B. Randall, J. Daniere, F. Guillet, Use of acceleration signal of a gearbox in order to perform angular resampling (with limited speed fluctuation), *Mechanical Systems and Signal Processing* 19 (4) (2005) 766–785.
[5] W.J. Staszewski, K. Worden, G.R. Tomilson, Time–frequency analysis in gearbox fault detection using the Wigner–Ville distribution and pattern recognition, *Mechanical Systems and Signal Processing* 11 (5) (1997) 673–692.
[6] W.J. Staszewski, G.R. Tomilson, Local tooth fault detection in gearboxes using a moving window procedure, *Mechanical Systems and Signal Processing* 11 (3) (1997) 331–350.
[7] W.J. Staszewski, G.R. Tomilson, Application of wavelet transform to fault detection in spur gear, *Mechanical Systems and Signal Processing* 8 (3) (1994) 289–307.
[8] W.J. Wang, P.D. McFadden, Early detection of gear failure by vibration analysis-I. Calculation of the time–frequency distribution, *Mechanical Systems and Signal Processing* 7 (3) (1993) 193–203.
[9] W.J. Wang, P.D. McFadden, Application of wavelets to gearbox vibration signals for fault detection, *Journal of Sound and Vibration* 192 (5) (1996) 927–939.
[10] C. Kar, A.R. Mohanty, Monitoring gear vibrations through motor current signature analysis and wavelet transform, *Mechanical Systems and Signal Processing* 20 (1) (2006) 158–187.
[11] C. Kar, A.R. Mohanty, Multi-stage gearbox condition monitoring through motor current signature analysis and Kolmogorov–Smirnov test, *Journal of Sound and Vibration* 290 (1–2) (2006) 337–368.
[12] G. Dalpiaz, A. Rivola, R. Rubini, Effectiveness and sensitivity of vibration processing techniques for local fault detection in gears, *Mechanical Systems and Signal Processing* 14 (3) (2000) 387–412.
[13] N. Byder, A. Ball, Detection of gear failures via vibration and acoustics signals using wavelet transform, *Mechanical Systems and Signal Processing* 17 (4) (2003) 787–804.
[14] H.A. Gaborson, The use of wavelets for analyzing transients machinery vibration, *Sound and Vibration* (2002) 12–17.
[15] L. Ran, R. Yacamini, K.S. Smith, Torsional vibrations in electrical induction motor drives during start-up, *Journal of Vibration and Acoustics—Transaction of ASME* 118 (1996) 242–251.
[16] H. Douglas, P. Pillay, A.K. Ziarani, A new algorithm for transient motor current signature analysis using wavelets, *IEEE Transactions on Industry Application* 40 (5) (2004) 1361–1368.
[17] H. Douglas, P. Pillay, The impact of wavelet selection on transient motor current signature analysis. *IEEE International Conferences on Electric Machines and Drives* (2005) 80–85.
[18] J. Antonino-Daviu, M. Riera-Guasp, J. Roger-Folch, F. Martínez-Giménez, A. Peris, Application and optimization of the discrete wavelet transform for the detection of broken rotor bars in induction machines, *Applied and Computational Harmonic Analysis* 21 (2) (2006) 268–279.
[19] L. Eren, M.J. Devany, Motor bearing damage detection via wavelet analysis of the starting current transient, *IEEE Instrumentation and Measurement Technology Conference* (2001) 1797–1800.
[20] S. Nandi, H.A. Toliyat, Novel frequency-domain-based technique to detect stator interturn faults in induction machines using stator induced voltages after switch-off, *IEEE Transactions on Industry Application* 38 (1) (2002) 101–109.
[21] R. Yacamini, K.S. Smith, L. Ran, Monitoring torsional vibrations of electro-mechanical systems using stator currents, *Journal of Vibration and Acoustics—Transactions of the ASME* 120 (1998) 72–79.
[22] B. Liang, S.D. Iwnicki, A. Ball, Asymmetrical stator and rotor faulty detection using vibration phase current and transient speed analysis, *Mechanical Systems and Signal Processing* 17 (4) (2003) 857–869.
[23] C. Kar, A.R. Mohanty, Gearbox health monitoring through multiresolution Fourier transform of vibration and current signals, *Structural Health Monitoring* 5 (2) (2006) 195–200.
[24] R. Schoen, T.G. Habetler, Effects of time-varying loads on rotor fault detection in induction machines, *IEEE Transactions on Industry Application* 31 (4) (1995) 900–906.
[25] H. Henao, H. Razik, G.A. Capolino, Analytical approach of the stator current frequency harmonics computation for detection of induction machine rotor faults, *IEEE Transactions on Industry Application* 41 (3) (2005) 801–807.
[26] H. Zheng, Z. Li., X. Chen, Gear fault diagnosis based on continuous wavelet transform, *Mechanical Systems and Signal Processing* 16 (2–3) (2002) 447–457.
[27] C. Kar, A.R. Mohanty, Time-varying parameters in vibration excitation of helical gears, *Proceedings of International Conference on Theoretical, Applied, Computational, and Experimental Mechanics*, IIT, Kharagpur, 2004, pp. 1–14.
[28] R. Schoen, T.G. Habetler, Evaluation and implementation of a system to eliminate arbitrary load effects in current-based monitoring of induction machines, *IEEE Transactions on Industry Application* 33 (6) (1997) 1571–1577.